OBSERVATIONS AND MAPPING OF SEDIMENTARY FEATURES NEAR SELECT

TESSERAE ON VENUS

By

SCOTT PETERSEN

_____

A Thesis Submitted to The W.A. Franke Honors College

In Partial Fulfillment of the bachelor's degree
With Honors in

Planetary Geoscience

THE UNIVERSITY OF ARIZONA

M A Y   2 0 2 5

Approved by:

Prof. Lynn Carter
Department of Planetary Sciences

Abstract

From spring 2024 to spring 2025, I worked with Professor Lynn Carter at the Lunar and Planetary Laboratory on a project to determine how tesserae on Venus interact with the planet's sedimentary cycle and associated processes. We produced a map sedimentary features that will be posted on the University of Arizona ReDATA repository in the coming weeks (University of Arizona, 2025). We also produced an abstract and poster presentation for the 56th Lunar and Planetary Science Conference (LPSC). We also adapted a dune crestline mapping algorithm from Telfer et al. (2015) to apply to dune fields on Earth to attempt to use the dune fields as analogs for microdunes on Venus. We found that sedimentary features near tesserae were somewhat rare. Nonetheless, we mapped the location of wind streaks, possible mass wasting, low emissivity terrain, and newly classified "outlines" in the immediate vicinity of several tesserae. We also discovered two microdune fields in Tellus tessera and Husbishag tessera. While we ran out of time to use our crestline mapping algorithm to study analogs of Venus microdunes, we were able to qualitatively determine that dune morphology does affect their appearance in SAR imagery depending on the direction they are imaged from.

1.　　Introduction

1.1　Data Sources

Most of the data in this project came from NASA's Magellan mission in the form of SAR imagery, though we also used the mission's radiometry data to characterize and map the low-emissivity terrain that sometimes occurred near mapped tesserae. Magellan acquired S-band horizontal transmit/horizontal receive (HH) SAR images that were either westward looking or eastward looking (Ford et al., 1993). These image sets are called "left look" and "right look" images, respectively. Image collection was done over several mission cycles, where each cycle represented a sidereal Venusian day (Ford et al., 1993). Cycle 1 was devoted to a global left-look map, Cycle 2 was a right-look map, and Cycle 3 was another left-look map, but at a different radar beam incidence angle with Venus's surface than in Cycle 1 to enable stereo image altimetry. Magellan's SAR resolution maximum was 75 m and varied with latitude, with the poles of Venus receiving the lowest resolution imagery. The mission's radiometer resolution was approximately 4 km (Ford et al., 1993). We also used Sentinel-1 SAR imagery for the Earth analog sites. Sentinel-1 uses a C-band radar imager (European Space Agency, 2025a), which is shorter wavelength than Magellan's S-band imagery. While Sentinel-1 imagery contains a variety of radar polarization information, we only used HH imagery.

1.2　Motivation and Literature Review

Tesserae are heavily tectonized regions on Venus characterized by the presence of at least two non-parallel tectonic fabrics and are generally older than all adjacent terrains (Ivanov and Head, 2011). They occupy approximately 7% of Venus's surface (Ivanov and Head, 2011). According to Gilmore et al. (2015), the tessera Alpha Regio may have a more felsic composition than the basaltic plains that dominate the rest of Venus's surface. The combination of these two facts is often used to interpret tesserae as being the oldest geologic units on Venus, and that they may record a different tectonic and climatic regime than present-day Venus (Gilmore et al., 2015). However, recent findings suggest that at least some tessera terrain may actually be

younger than adjacent terrain and could be actively forming out of basaltic plains material (Byrne et al., 2022).

Characterizing tesserae could help to constrain the ways that they form and help in understanding tectonics on Venus. If some tessera terrain was indeed formed in Venus's deep past, they may hold information about Venus's evolution. This work is intended to increase understanding of tesserae by providing a map of sedimentary features in the vicinity of several tesserae. The map is intended primarily to aid in targeting the VenSAR instrument aboard the EnVision spacecraft. VenSAR is expected to have a maximum resolution of 10 m per pixel (European Space Agency, 2025b), which is approximately an order of magnitude greater than Magellan's maximum resolution. As VenSAR will be mapping pre-selected targets on Venus's surface, helping to determine the most useful sediment/tessera-related sites will aid in maximizing the gain in understanding of tesserae's relationship to sediments on Venus.

Our study of sediments near Venusian tesserae was motivated by peculiar findings of previous works. Byrne et al. (2021) had found that some tessera terrain resembles eroded mountain belts on Earth, which they suggested means that there has been extensive erosion of Venus's tessera. In addition, Ganey et al. (2023) found that the global volume of visible sediment on Venus is less than what should be expected based on sediment generated by impacts. However, they also found that specific aeolian features had a greater volume of sediment than locally available from nearby impact craters, implying either long-range sediment transport on Venus or an unknown sediment source (or both). The issue of a lack of sediment on a global scale is possibly mitigated by Bondarenko and Kreslavsky (2018)'s findings, where their principal component of analysis of Magellan SAR imagery and radiometry indicated that much of Venus may be covered in a mantle of sediment that is invisible in the Magellan SAR imagery. Finally, Campbell et al. (2015) and Whitten and Campbell (2015) both found and mapped crater ejecta occurring on the tessera Alpha Regio, but not on adjacent plains, suggesting that the tessera inhibited the weathering of the ejecta. The combination of these findings strongly indicates that tessera terrain plays an important role in Venus's sediment cycle, but an exact characterization of this role remains somewhat unconstrained.

1.3   Microdunes

A class of sedimentary feature on Venus that we investigated in detail are the so-called "microdunes." This term was introduced by Weitz et al. (1994), who first discovered them. Microdunes are asymmetric aeolian bedforms or dunes that are smaller than the resolution limit of Magellan SAR imagery. Because they are asymmetrical, if they are oriented nearly perpendicular to Magellan's radar beam, they can cause terrain to have drastically different radar cross-sections between opposing radar beam directions. To control for the effect of the variable incidence angle of Magellan's radar beam, which would affect the observed radar cross-section of the terrain at a given latitude, only the latitudes where Magellan's right- and left-looking imagery have the same approximate absolute value of incidence angle can be used to search for microdunes (Weitz et al., 1994).

2.   Methods

2.1   Mapping

Mapping of Venus was done in ArcGIS Pro (Esri, 2025). Magellan imagery was acquired from the online USGS Astropedia tool (USGS..., n.d.). The images were sections of the full resolution Magellan SAR data records resampled at a 75 m resolution. Section bounds were determined by using Ivanov and Head (2011)'s geologic map of Venus, which allowed us to acquire imagery of our target tesserae with an approximately 0.3 degree padding. We prioritized mapping tesserae that had coverage from multiple imaging cycles to maximize our ability to interpret observed features. Figure 1 shows a map of all of the regions we mapped.
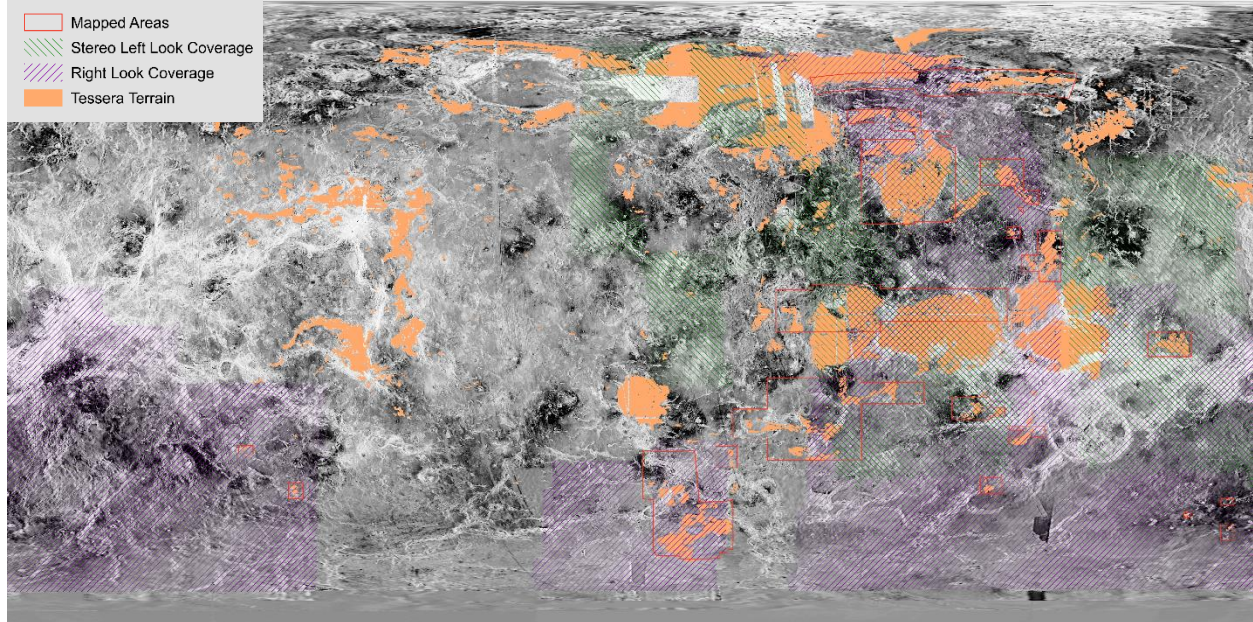

Figure 1: *A map of Venus showing the extent of our mapping campaign. Area classified as tessera terrain by Ivanov and Head (2011) is filled in with light orange. Regions covered by stereo left look and right look imagery are highlighted. The background map is a mosaic of all image cycles, but mainly the left-looking Cycle 1 (USGS..., n.d.). This figure was presented in our poster at the 56th LPSC.*

Mapping was conducted by manually scanning back and forth across an image section at 1:400,000 scale. At this scale, individual pixels were visible. When a suspected sedimentary feature was encountered, it would be outlined according to its classification and added to an ArcGIS Feature Class. The image stretch of each section was adjusted to be a histogram with the top and bottom 1% of the data clipped based on the backscatter histogram of Tellus Regio. This image stretch was copied to all image sections to maximize consistency in interpretation. However, certain sections (such as Ovda Regio) contained especially radar-bright or radar-dark terrain, which necessitated temporarily altering the image stretch so they could be adequately mapped. The map projection was also changed near the poles of Venus to reduce geometric distortions. Features were identified manually based on comparison to past works, especially Greeley et al. (1995) for wind streaks and Malin (1992) for mass wasting. As mapping progressed, a greater diversity of features were sampled and classified. As a result, not all mapped tesserae contain each class of feature; however, this does not mean that certain

features are absent near specific tesserae. For example, the bright and dark outlines were only characterized as a distinct feature relatively late in the mapping process, so tesserae mapped earlier generally are not indicated to have these features, even though they may still be present. All mapped features were exported from ArcGIS in various file formats to be read by any GIS software (see section 3.1).

2.2   Microdune Analysis

The only property of microdunes that can be measured in SAR images is the difference in backscatter between two look directions. As they are subresolution features, their morphology is impossible to directly determine without higher resolution imagery. We hoped to indirectly infer some of the microdunes' properties by determining how the morphology of dune fields on Earth affect their change in backscatter when viewed from different directions. Blom and Elachi (1981) have previously investigated the effects of incidence angle and look direction on the dune fields in SAR images, finding the backscatter to be sensitive to both of those factors.

We used Sentinel-1 C-band SAR images from opposite look angles acquired from ESA's online Copernicus system (European Space Agency, 2025c). Due to time constraints, we were only able to investigate the dune field at White Sands National Park. This dune field was chosen because the dune crestlines are roughly perpendicular to Sentinel-1's radar beam, and based on Blom and Elachi (1981)'s findings, this should mean that the change in backscatter from right- and left-looking images should be most pronounced. Raw SAR images were processed in ArcGIS Pro (Esri, 2025) to be converted from digital number values to radar cross section values. ArcGIS Pro's Geometric Terrain Correction tool was applied using a USGS DEM with 8 m horizontal resolution (US Geological Survey 2025a; 2025b). This unfortunately removed distortion from topography, but still maintained changes in backscatter due to local incidence angle. Attempts to georeference the radar imagery without using the Geometric Terrain Correction tool were unsuccessful.

To attempt to quantitatively analyze the morphology of the White Sands dunes we adapted an automatic dune crestline mapping algorithm from Telfer et al. (2015). Direct application of their algorithm was unsuccessful to optical orbital imagery, so we instead used the USGS's Digital Elevation Models (DEMs). Pixels in the DEM were classified as being a likely crestline if they satisfied the following inequality from Telfer et al. (2015) taken over a moving window: $P > \alpha x + a\sigma$, where P is the value of the slope of the DEM at a given pixel, x is the mean value of pixels in the window, σ is the standard deviation of the pixel values, and α and a are constants. 52 permutations of window size, α, and a were tested to determine which combination was best at identifying crestlines. A 15x15 pixel window with $\alpha = 0.5, a = 1.5$ yielded the best results as determined by visual inspection.

Following Telfer et al. (2015), we computed the direction of the slope of the DEM for each pixel to eliminate all pixels outside of ±90° of the heading corresponding to the average crestlines. This is possible as there were strong peaks in the histogram of slope direction pixels that corresponded to the lee and stoss sides of all of the dunes. Using the statsmodels python package's Kernel Density Estimator (Perktold et al., 2025), we were able to extract the modal peak corresponding to the lee side of the dunes. This allowed us to mask out all stoss-side pixels that had been classified as being part of a crestline. The resulting raster of crestline pixels was exported to Adobe Illustrator where we used its Image Trace tool to vectorize the raster (Adobe,

2025). Image Trace mode was set to "Black and White," noise to 2 pixels, path to 100%, corners to 90%, and threshold to 254. Then, to enable the curved geometry to be imported properly into ArcGIS, we ran Illustrator's "Add Anchor Points" tool on the vectorized crestline map five times. The entire crestline map was then scaled down, assuming one pixel corresponded to one degree, and moved to pixel coordinates approximately corresponding to White Sands National Park. ArcGIS is unable to accept .svg files, so we instead imported the vectorized crestline map as a .dwg file. After converting the resulting CAD Layer to a Feature Class, we moved and scaled the vectorized map of crestlines until it overlapped with the dunes. Further analysis may require code to decompose the feature class into individual polylines, which we did not develop. We were also unable to complete an analysis and comparison of White Sands's dunes to Venus's microdunes due to time constraints.

3.   Results

3.1   Description of Mapping Data

Our mapping campaign yielded 11 classes of sedimentary features covering a total area of 3.38×10^7 km^2, or approximately 7% of Venus' surface. The following sections describe each class in detail, with each section title being the name of the corresponding .shp file.
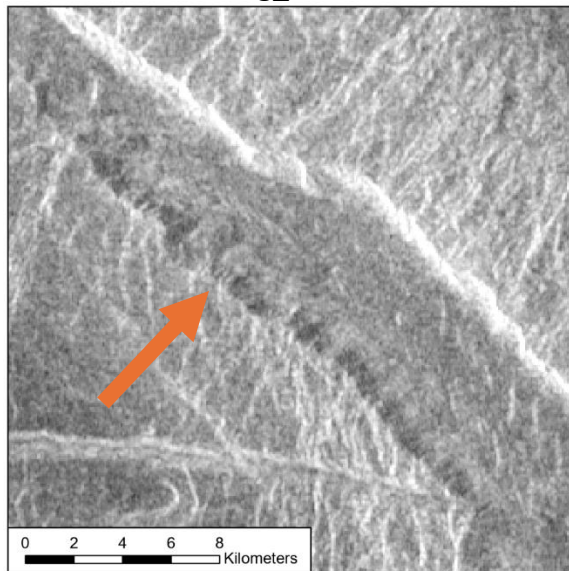
3.1.1   MassWasting_LowConfidence

Figure 2: An instance of Mass Wasting, Low Confidence in Gegute tessera at 116.608°N, 14.026°W. Radar beam illumination is from the left. Note the bright-dark-bright pattern where the arrow is pointing.

Features in Mass Wasting, Low Confidence are suspected instances of mass wasting but are too small to be confidently interpreted as such. These features were identified based on the presence of lobe shapes, a pattern of dark-bright-dark on slopes facing away from the radar beam, or visual similarity to talus slopes as pictured in Malin (1992) and Carter (2023). These features occur frequently in graben near tesserae but are rare within or on the margins of tesserae. We believe the dark-bright-dark pattern is the result of roughening on the scale of Magellan's radar wavelength occurring at the base of a slope due to the presence of talus deposits.

3.1.2 MassWasting_HighConfidence

These features are also suspected instances of mass wasting but are large enough to allow a highly confident interpretation as mass wasting. Most instances of this class of feature are more related to coronae or chasmata than tesserae, which is supported by Jesina et al. (2025)'s discussion of mass wasting as a tracer for seismic activity.

3.1.3 Pits

This class of feature refers to any chain of pits observed. There would often be instances of mass wasting, low confidence on the walls of the largest pits. We interpreted these mostly as volcanic dikes breaching the surface or as incipient graben. They occurred frequently within and outside of tesserae, often in association with intratessera plains.
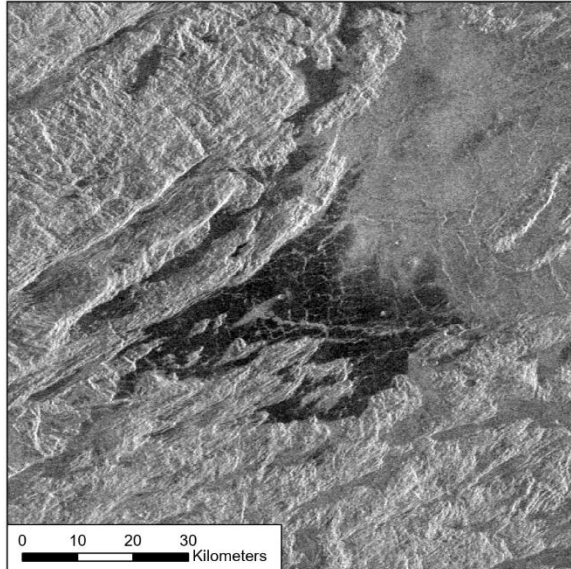
3.1.4 Dark_LowEpsilon

Figure 3: An example of a low epsilon dark feature adjacent to and slightly overlapping with Kutue tessera at 39.339°N, 107.290°E. Both well-defined and diffuse margins are present on this instance. Radar illumination is from the right.

These features were characterized by the presence of radar dark terrain and a high emissivity as measured by Magellan's radiometer. We used Magellan's global emissivity map (Magellan Team, 1993) to derive a global map of the surface dielectric constant using the methodology presented in Ford et al. (1993). The globally averaged surface dielectric constant of Venus is approximately 4 (Pettengill et al., 1992), while the emissivity-derived dielectric constant in Dark Low Epsilon features was generally between 2 and 2.5 (where "epsilon" refers to the dielectric constant). According to Ford et al. (1993), rougher surfaces generally have a higher emissivity. However, the very low backscatter implies that the deposits are smooth. This implies that these features may be very low density, like a sediment mantle. The margins of features in this class varied from very well-defined to diffuse. Instances of low epsilon dark tended to obscure tectonic fabrics.

3.1.5 Wind Streaks

Wind streaks were fairly abundant, though it was very rare for any to be emanating from a tessera. Wind streaks were subdivided into five classes based on Greeley et al. (1995)'s classification scheme for wind streaks. Several streaks had also been previously noted by Greeley et al. (1995), but we were unable to verify exactly which ones due to difficulty precisely georeferencing their maps.

Streaks_Linear_Sparse

Greeley et al. (1995) had a single category for "linear streaks," however we decided to split this category into "sparse" and "dense" subclasses. The sparse linear streaks were characterized by having a length to width ratio significantly greater than the topographic feature they were attached to and not being directly attached to other wind streaks.

Streaks_Linear_Dense

Dense linear streaks are streaks that occur in a very closely packed group but are still resolvable as individual streaks with high length to width ratios. As noted in Greeley et al. (1995), these streaks can be so densely packed that it becomes difficult to determine if the streaks are radar bright and the underlying terrain is radar dark, or vice versa.

Streaks_Transverse

Streaks of this class were identified based on criteria identical to the transverse streaks in Greeley et al. (1995). They always occurred immediately adjacent to a linear topographic feature. While they could cover the same area as a dense linear streak, they were not composed of many individual streaks and instead were a continuous covering of radar bright or dark material.

Streaks_Wispy

Wispy streaks were also classified the same way as in Greeley et al. (1995). These streaks had meandering, linear forms and could approach lengths of 100 km. They often seemed to be approximately perpendicular to nearby streaks, though it seems their directionality was mainly controlled by the presence of topographic features, as was also the case in Greeley et al. (1995).

Streaks_Fan

Fan streaks were any streaks that occurred adjacent to shield volcanoes. While Greeley et al. (1995) had a broader characterization of fan streaks as any streak that occurred in isolation with a length to width ratio smaller than 20:1, we only qualitatively noted the length to width ratio of all streaks. However, the streaks we classified as fan streaks had very small length to width ratios, often not being longer than the source shield volcano while being just as wide. These were only observed on plains terrain near tesserae, though it is possible that some of the shield volcanoes we observed occurring within tessera terrain also had fan streaks that were masked by the complicated geometry and high backscatter of the tessera.
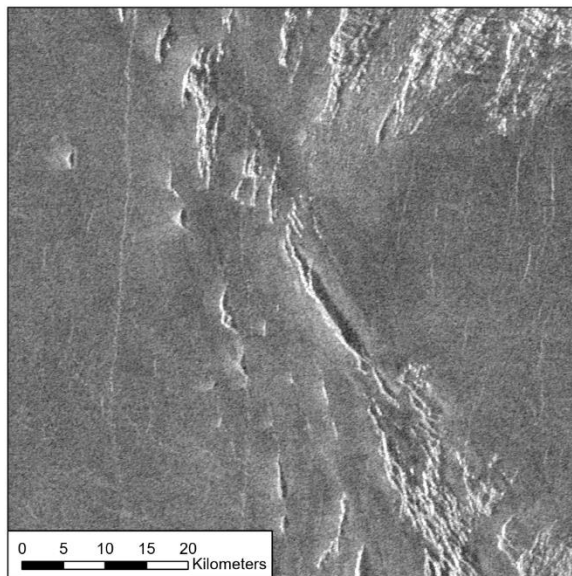
3.1.6   Outlines

Figure 4: This was one of the densest clusters of bright outlines, occurring at 56.373°S, 20.522°E in Cocomama tessera. Note that the bright outlines wrap around several tessera outcrops. Radar illumination is from the left.
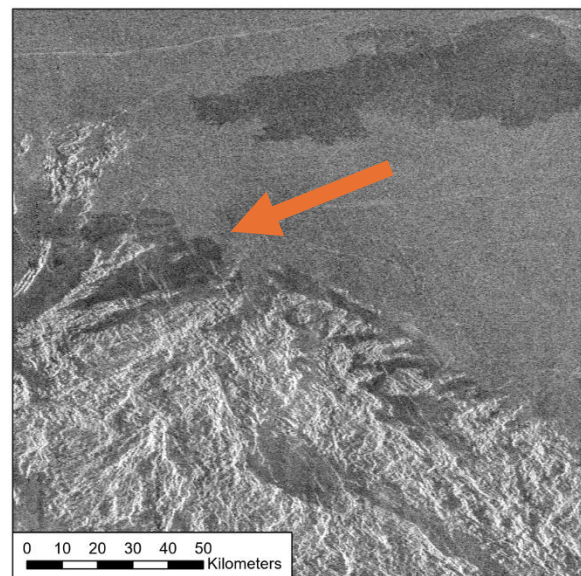
Figure 5: An example of a dark outline, indicated by the arrow. This outline also occurred in Cocomama tessera, at 58.271°S, 23.952°E. It is unclear if the dark lava flow is related. Radar illumination is from the left.

Outlines are features we define as a diffuse radar bright or radar dark patch of terrain on the margins of a topographical feature. They are not a result of backscatter changing due to

topography as they persist in the same locations in both left- and right-look imagery. While they share some similarities with transverse streaks such as their diffuse form and appearance next to topography, they do not seem to have any directional characteristics other than that they fade farther from their host topographical feature. They can also range from being intermittent along a margin to fully surrounding a topographical feature. We divided them into two subclasses based on their radar brightness relative to the surrounding terrain: bright outlines and dark outlines.

Outlines_Bright

Bright outlines, shown in Figure 4, were often near instances of Mass Wasting, Low Confidence. They occasionally had nearly identical characteristics to Mass Wasting, Low Confidence, but were still classified as outlines due to the qualitatively larger distance the radar bright region extended. There were also several instances, such as the ones pictured in Figure 4, where the outlines only featured the diffuse brightness around a topographic margin.

Outlines_Dark

Dark outlines, pictured in Figure 5, sometimes occurred in association with transverse or dense linear streaks. Such instances of dark outlines may just be an unusual expression of those features. Like bright outlines, dark outlines were mainly found on tessera margins, though unlike bright outlines, they very frequently occurred in proximity to wind streaks. Dark outlines also sometimes share Dark Low Epsilon features' low dielectric constant but were not classified as such because they were not as dark.

3.2 Microdunes

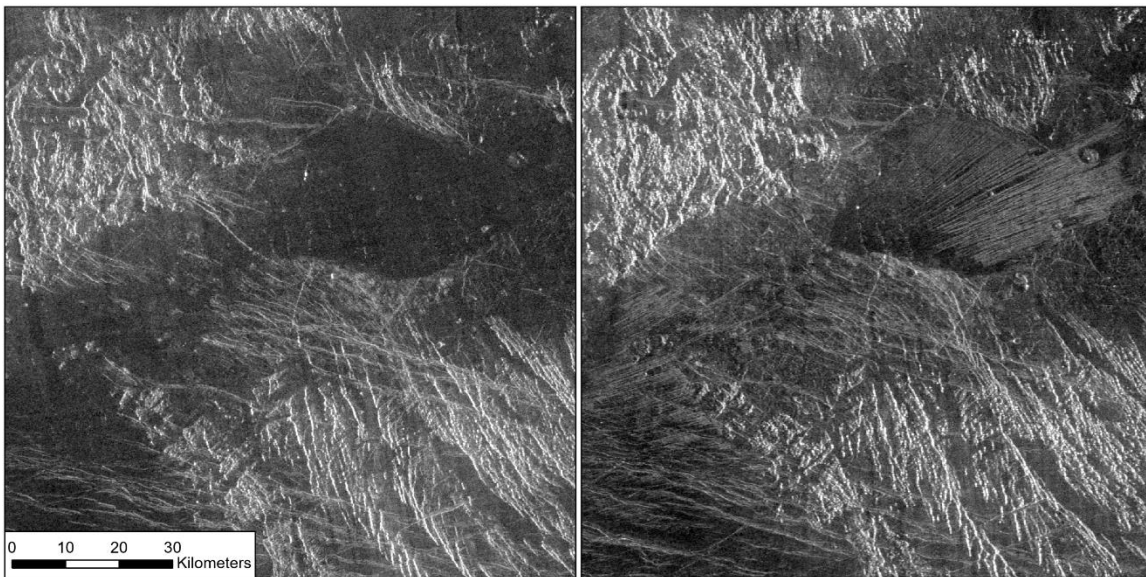### 3.2.1 Two New Microdune Fields

Figure 6: A side-by-side comparison of left-look (at left) and right-look (at right) SAR images. This image pair is of the highly structured microdunes discovered in Husbishag tessera at 29.804°S, 97.751°E.
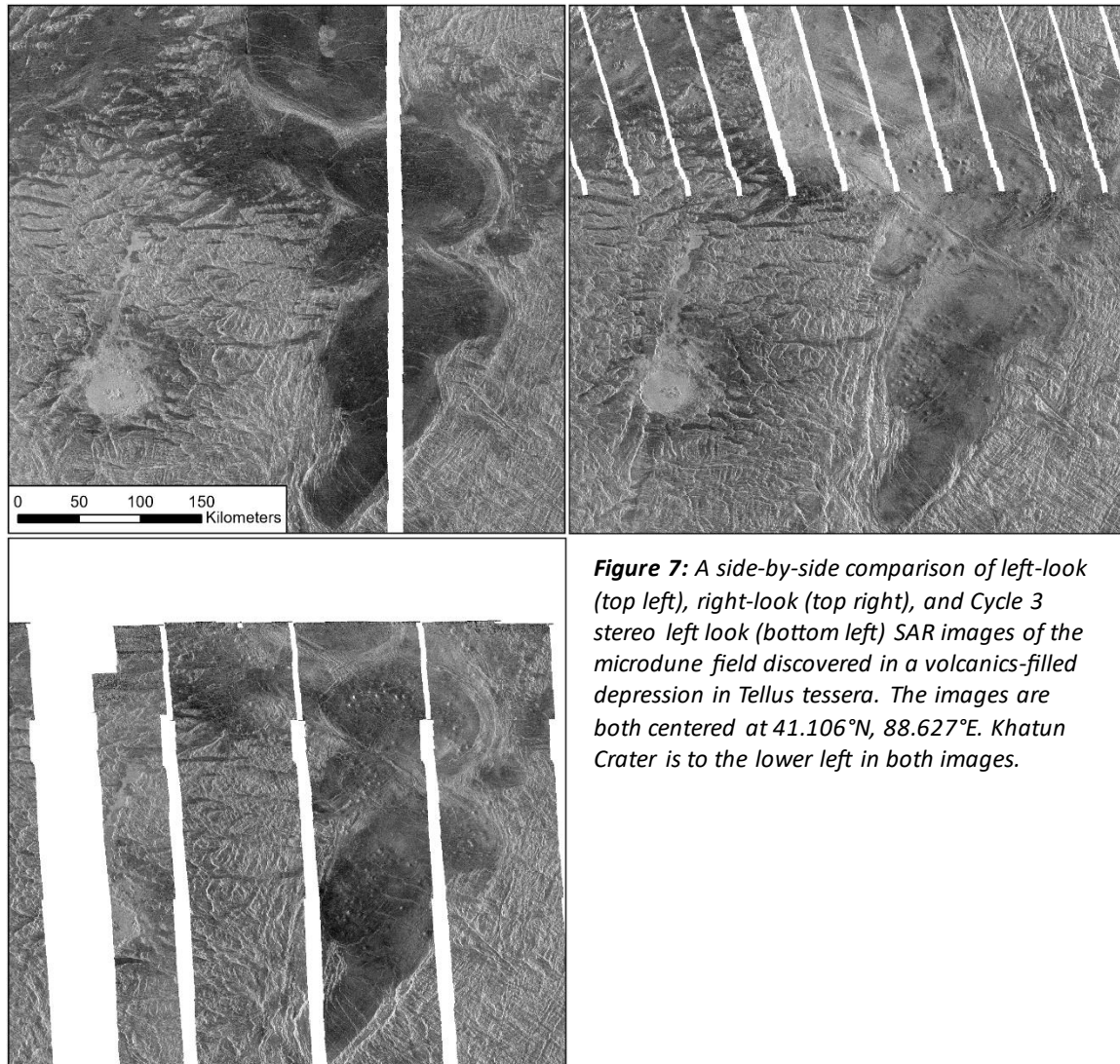
Figure 7: A side-by-side comparison of left-look (top left), right-look (top right), and Cycle 3 stereo left look (bottom left) SAR images of the microdune field discovered in a volcanics-filled depression in Tellus tessera. The images are both centered at 41.106°N, 88.627°E. Khatun Crater is to the lower left in both images.

Two new microdune fields were discovered during our mapping campaign. The first, shown in Figure 7, was in Tellus tessera. The difference in absolute value of incidence angle between Cycle 1 left-look and right-look images is too great to be useful for detecting microdunes according to Weitz et al. (1994). However, the difference of the absolute value is less than 5° between Cycle 3 left-look and right-look images (Ford et al., 1993), which means changes in brightness are likely not attributable to the change in incidence angle and thus must be from some asymmetric feature on the surface. This leads us to conclude that this is a microdune field. The average increase in brightness was about 2 dB between Cycle 3 left-look and right-look images within the volcanic depression.

We also discovered a microdune field in Husbishag tessera, shown in Figure 6. While the difference in absolute value of incidence angle between left- and right-looking images is greater than 10° at this latitude (Ford et al., 1993), we still believe that this feature is a microdune field. The dense linear streak-like features in Figure 6 only appear in right-looking images, and no trace of them exists in the left-looking images. This strongly implies that the streaks are

composed of small, asymmetrical features that have their lee side pointed to the right, allowing them to be invisible in left-looking images but striking in right-looking images.

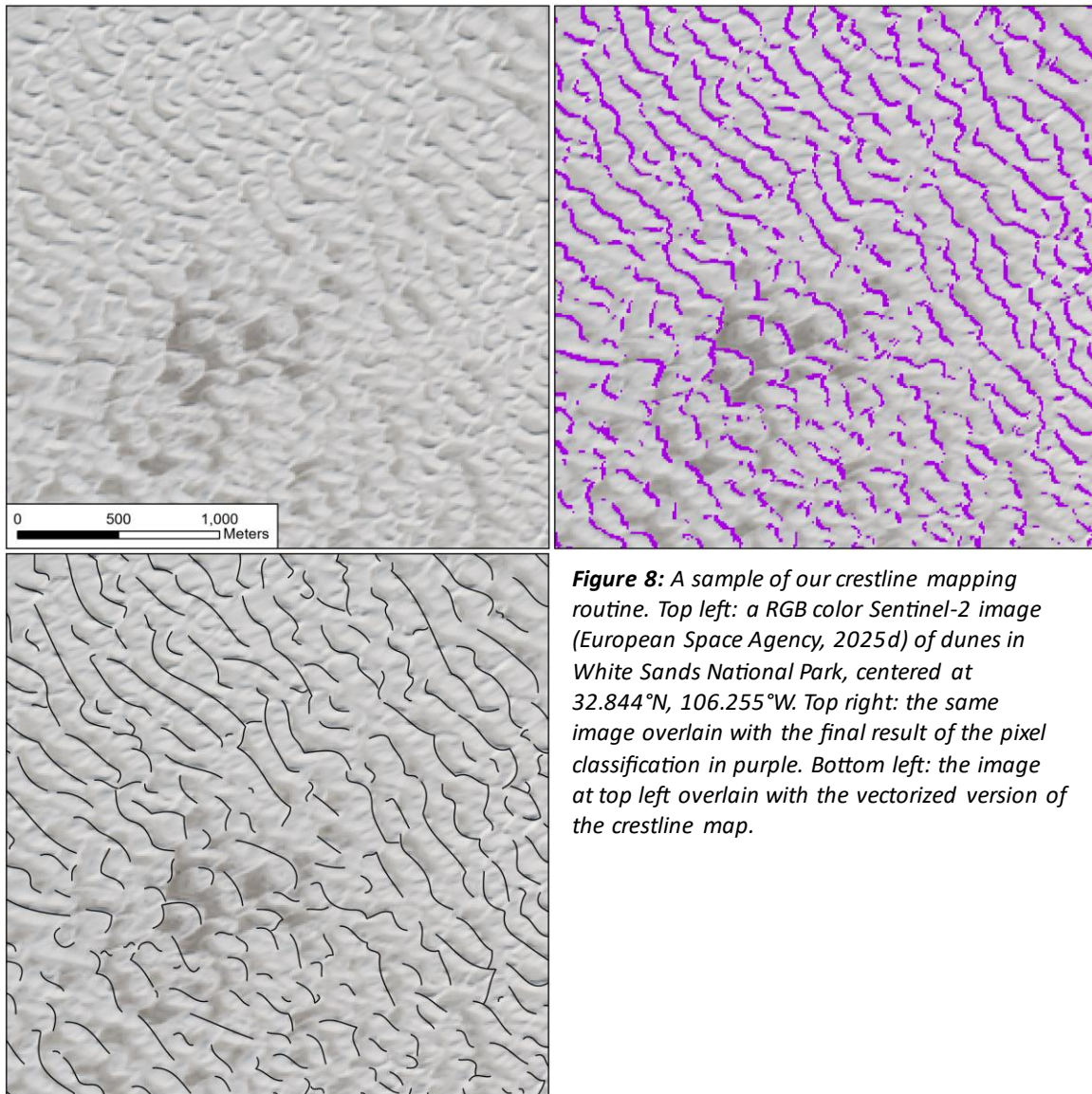### 3.2.2 Analog Comparison using White Sands National Park

Figure 8: A sample of our crestline mapping routine. Top left: a RGB color Sentinel-2 image (European Space Agency, 2025d) of dunes in White Sands National Park, centered at 32.844°N, 106.255°W. Top right: the same image overlain with the final result of the pixel classification in purple. Bottom left: the image at top left overlain with the vectorized version of the crestline map.

As explained in Section 2, we developed a routine to automatically map dune crestlines from a DEM based on Telfer et al. (2015)'s work. We were unable to analyze the dune field characteristics or apply the mapping routine to other dune fields, and as such were not able to determine the morphological properties that most affect changes in dune fields' radar backscatter. However, our crestline mapping routine is close to being usable. As can be seen in Figure 8, the vectorized version of the raster map of the crestlines tends to oversimplify the shape of the crestlines. Additionally, there are many stray lines that do not correspond to crestlines. The raster version of the crestline map (the purple in Figure 8) is, however, very close to correctly mapping the crestlines. Thus, we believe that some adjustments to the vectorization step of our routine will allow it to yield useful and usable results.

4. Discussion and Conclusion

This project led to the creation of a map of sedimentary features near tesserae on Venus, the discovery of two new microdune fields on Venus, and extensive development of an automated dune field crestline mapping routine. We hope that this work will help support the VenSAR and EnVision teams by facilitating targeting of sedimentary features, and possibly enabling future work on aeolian Earth analogs for Venus.

5. Data and Code Availability

Shapefiles for the sedimentary map will be posted on ReDATA (University of Arizona, 2025) in the next few weeks. The code for the crestline mapping routine will also be posted to the same ReDATA repository. These two items are currently available on a GitHub repository at https://github.com/ScottyP123/Observations-and-Mapping-of-Sedimentary-Features-near-Select-Tesserae-on-Venus.

6. Acknowledgements

6. References

Adobe. (2025). *Adobe Illustrator* (Version 29.5) [Computer Software]. https://www.adobe.com/products/illustrator.html

Blom, R., Elachi, C. (1981). Spaceborne and Airborne Imaging Radar Observations of Sand Dunes. *Journal of Geophysical Research*, 86:B4, Pp. 3061-3073. Doi: https://doi.org/10.1029/JB086iB04p03061

Bondarenko, N. V., Kreslavsky, M. A. (2018). Surface properties and surficial deposits on Venus: New results from Magellan radar altimeter data analysis. *Icarus*, 309, Pp. 162-176. Doi: https://doi.org/10.1016/j.icarus.2018.03.013

Byrne, P. K., Ghail, R. C., James, P. B., Klimczak, C., Celâl Şengör, A. M., Solomon, S. C. Recent and Possibly Ongoing Formation of Tesserated Rocks on Venus. (2022). *53rd Lunar and Planetary Science Conference*, Abstract 1197. https://www.hou.usra.edu/meetings/lpsc2022/pdf/1197.pdf

Carney, Stephen. (2024). *Magellan*, National Aeronautics and Space Administration. https://science.nasa.gov/mission/magellan/

Carter, L. M., Gilmore, M. S., Ghail, R. C., Byrne, P. K., Smrekar, S. E., Ganey, T. M., Izenberg, N. (2023). Sedimentary Processes on Venus. *Space Science Reviews*, 219:85. Doi: https://doi.org/10.1007/s11214-023-01033-2

Esri. (2025). *ArcGIS Pro* (Version 3.2.0) [Computer Software]. https://pro.arcgis.com/en/pro-app/latest/get-started/get-started.htm

Ivanov, M. A. Head, J. W. (2011). Global geological map of Venus. *Planetary and Space Science*, 59. Pp. 1559-1600. Doi: 10.1016/j.pss.2011.07.008.

Gilmore, M. S., Mueller, N., Helbert, J. (2015). VIRTIS emissivity of Alpha Regio, Venus, with implications for tessera composition. *Icarus*, 254. Pp. 350-361. Doi: http://dx.doi.org/10.1016/j.icarus.2015.04.008

European Space Agency. (2025a). *S1 Mission: Overview of Sentinel-1 Mission*. https://sentiwiki.copernicus.eu/web/s1-mission

European Space Agency. (2025b). *VENSAR*. https://www.cosmos.esa.int/web/envision/vensar#

European Space Agency. (2025c). Copernicus Space Data Ecosystem Browser. https://browser.dataspace.copernicus.eu

European Space Agency. (2025d). *Sentinel-2*. https://dataspace.copernicus.eu/explore-data/data-collections/sentinel-data/sentinel-2

Ford, J. P., Plaut, J. J., Weitz, C., Farr, T. G., Senske, D. A., Stofan, E. R., Micheals, G., Parker, T. J. (1993). Guide to Magellan Image Interpretation. JPL Publication 93-24. https://ntrs.nasa.gov/citations/19940013181

Ganey, T. M., Gilmore, M. S., Brossier, J. (2023). Reassessment of the Volumes of Sediment Sources and Sinks on Venus. *The Planetary Science Journal*, 4:9. Doi: https://doi.org/10.3847/PSJ/aca521

Greeley, R., Bender, K., Thomas, P. E., Schubert, G., Limonadi, D., Weitz, C. (1995). Wind-Related Features and Processes on Venus: Summary of Magellan Results. *Icarus*, 115, Pp. 399-420. Doi: https://doi.org/10.1006/icar.1995.1107

Jesina, E. L., Carter, L. M., Ganesh, I. (2025) Identifying Landslides in Atla Regio on Venus. *Journal of Geophysical Research: Planets*, 130:4. Doi: https://doi.org/10.1029/2024JE008453

Malin, M. (1992). Mass Movements on Venus: Preliminary Results from Magellan Cycle I Observations. *Journal of Geophysical Research*, 97:10, Pp. 16337-16352. Doi: https://doi.org/10.1029/92JE01343

Perktold, J., Seabold, S., Taylor, J. (2025). *statsmodels: Kernel Density Estimation* (Version 0.15.0) [Computer Software]. https://www.statsmodels.org/dev/examples/notebooks/generated/kernel_density.html

Petersen, S. K., Carter, L. M. (2025). Preliminary Observations of Sedimentary Processes near Venusian Tesserae. *56th Lunar and Planetary Science Conference*, Abstract 1823. https://www.hou.usra.edu/meetings/lpsc2025/pdf/1823.pdf

Pettengill, G. H., Ford, P. G., Johnson, W. T. K., Raney, R. K., Soderblom, L. A. (1992). Venus Surface Radiothermal Emission as Observed by Magellan. *Journal of Geophysical Research*, 97, Pp. 13091-13102. Doi: https://doi.org/10.1029/92JE01356

Telfer, M. W., Fyfe, R. M., Lewin, S. Automated mapping of linear dunefield morphometric parameters from remotely-sensed data. *Aeolian Research*, 19, Pp. 215-224. Doi: http://dx.doi.org/10.1016/j.aeolia.2015.03.001

The Magellan Team and Ford, P., Pettengill, G., Liu, F., Quigley, J. (1993). Venus Magellan Global Microwave Emissivity 4641m. *USGS Astrogeology Science* Center. https://astrogeology.usgs.gov/search/map/venus_magellan_global_microwave_emissivity_4641m

University of Arizona. (2025). *ReDATA*. https://redata.arizona.edu/

USGS Astrogeology Science Center. (n.d.). *Astropedia: Lunar and Planetary Cartographic Catalog*. https://astrogeology.usgs.gov/search?target=Venus&system=&p=1&accscope=&searchBar=

US Geological Survey. (2024a). USGS 1/3 Arc Second n34w107 20240416. https://www.sciencebase.gov/catalog/item/6627419bd34ea70bd5efaed4

US Geological Survey. (2024b). USGS 1/3 Arc Second n33w107 20240416. https://www.sciencebase.gov/catalog/item/662741abd34ea70bd5efaee6

Weitz, C. M., Plaut, J. J., Greeley, R., Saunders, R. S. (1994). Dunes and Microdunes on Venus: Why Were So Few Found in the Magellan Data? *Icarus*, 112, Pp. 282-295. Doi: https://doi.org/10.1006/icar.1994.1181